High-performance near-infrared (NIR) polymer light-emitting diodes (PLEDs) based on bipolar Ir(III)-complex-grafted polymers

Wentao Li,‡[a] Baowen Wang,‡[a] Tiezheng Miao,[a] Jiaxiang Liu,[a] Guorui Fu,[a,c*] Xingqiang Lü[a,*] Weixu Feng[b,*] and Wai-Yeung Wong[c,*]

Despite the cost-effective and large-area scalable advantages of NIR-PLEDs based on iridium(III)-complex-doped polymers, the intrinsic phase-separation issue leading to inferior device performance is difficult to be addressed. In this study, taking the vinyl-functionalized **[Ir(iqbt)$_2$(vb-ppy)]** (**Hqibt** = 1-(benzo[*b*]-thiophen-2-yl)-isoquinoline; **vb-Hppy** = 2-(4′-vinylbiphenyl-4-yl)pyridine) as the polymerized complex monomer, two series of Ir(III)-complex-grafted polymers **Poly(NVK-*co*-[Ir(iqbt)$_2$(vb-ppy)])** and **Poly((vinyl-PBD)-*co*-NVK-*co*-[Ir(iqbt)$_2$(vb-ppy)])** (NVK = *N*-vinyl-carbazole; **vinyl-PBD** = 2-(4-(*tert*-butyl)phenyl)-5-(4'-vinyl-[1,1'-biphenyl]-4-yl)-2,5-dihydro-1,3,4-oxadiazole) are obtained, respectively. Moreover, by using the bipolar Ir(III)-complex-grafted polymer further doped or grafted with electron-transport unit as the emitting layer (EML), their reliable NIR-PLEDs are realized. Especially based on the concurrent covalent-linkages of both the Ir(III)-complex and the **vinyl-PBD** towards the carrier-balanced **NIR-PLED-III**, the achievement of an almost negligible (< 5%) efficiency roll-off does not sacrifice the attractive efficiency (η_{QE}^{max} = 3.6%). This finding engenders bipolar Ir(III)-complex-grafted polymers a good platform to high-performance NIR-PLEDs.

1. Introduction

Driven by the promising applications of near-infrared (NIR) organic/polymer light-emitting diodes (NIR-OLEDs/PLEDs) in night-vision and information-security displays,[1] telecommunications[2] and photo-dynamic therapies,[3] concerted efforts have been devoted to the development of new and efficient NIR-emitters. In this context, owing to the harvesting of both singlet and triplet excitons towards a theoretical η_{lQE} (internal quantum efficiency) of 100%, NIR-emissive transition-metal (Pt(II), Ir(III) or Os(II), etc.) complex phosphors[4] together with TADF (thermal activated delayed fluorescence) molecules[5] capable of the facilitated reverse intersystem crossing (RISC), are highly attractive. Saliently regarding the octahedral Ir(III)-complexes with rather short triplet lifetimes, high efficiency which is competitive to those of other triplet-utilized counterparts, together with the superiority of a significantly alleviated efficiency roll-off, engenders a particular appeal to their NIR-OLEDs/PLEDs.

Till now, concrete C^N-cyclometalated Ir(III)-complexes possessing neutral [Ir(C^N)$_3$]-homoleptic[6] or [Ir(C^N)$_2$(L^X)]-heteroleptic (L^X = O^O[7] or N^O[8]) and cationic [Ir(C^N)$_2$(N^N)]$^+$ forms,[9] were demonstrated for reliable NIR-OLEDs/PLEDs, and the wavelength-η_{EQE} (external quantum efficiency) relationship is summarized in **Figure 1** and **Table S1**. Nonetheless, as constrained by the so-called "energy gap law",[10] it remains a real challenge to develop new Ir(III)-complex-based NIR-emitters to achieve high efficiency. On the other hand, to suppress the detrimental triplet-triplet annihilation (TTA)[11] of the Ir(III)-complex-based phosphors with narrow HOMO-LUMO band-gaps for the NIR emissions, it is necessary and also challenging to dope one specific Ir(III)-complex into an appropriate small-molecule host for the vacuum-deposited/solution-processed NIR-OLED (NIR-OLEDs-V/S) or polymeric matrix for the NIR-PLED (**Table S1** and **Figure 1**), respectively. In comparison, although cost-effective solution-processed NIR-PLEDs with Ir(III)-complex-doped polymers as the EMLs are more advantageous for the large-area scalability, the simple doping suffers from an inevitable phase-separation issue,[12] thereby leading to inferior device efficiency and serious efficiency roll-off. Noticeably, despite the certain efficiency progress appreciable from the supplementation of one electron-transport

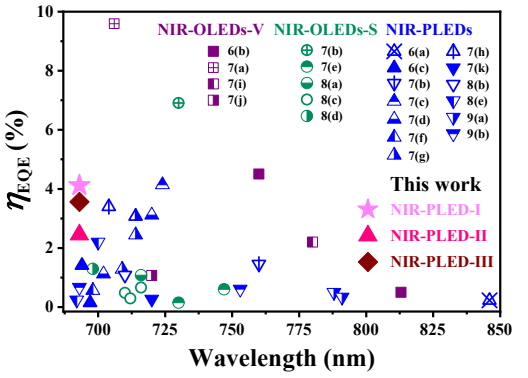

Figure 1. The λ_{em}-relative η_{EQE} comparison between the **NIR-PLEDs-I-III** in this work with those from Ir^{3+}-complexes doping in small-molecular or polymer host with vacuum-deposition (NIR-OLEDs-V) or solution-processing (NIR-OLEDs-S/PLEDs).

[a]*School of Chemical Engineering, Northwest University, Xi'an 710069, Shaanxi, China. E-mail: lvxq@nwu.edu.cn*
[b]*School of Chemistry and Chemical Engineering, Northwestern Polytechnical University, Xi'an 710029, Shaanxi, China. E-mail: fwxdk@nwpu.edu.cn*
[c]*Department of Applied Biology and Chemical Technology, The Hong Kong Polytechnic University, Hung Hom, Hong Kong, China. E-mail: guorui.fu@polyu.edu.qk; wai-yeung.wong@polyu.edu.hk*

‡These authors contributed equally and should be considered *co*-first authors.

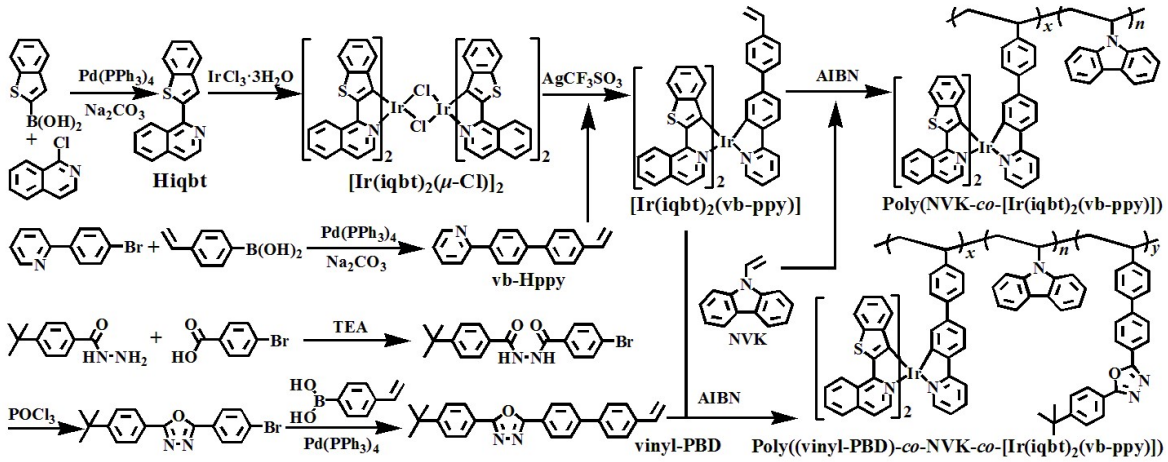

Scheme 1. Synthetic scheme of the ligands **Hiqbt**, **vb-Hppy**, **vinyl-PBD**, the complex monomer [**Ir(iqbt)$_2$(vb-ppy)]** and their two series of Ir^{3+}-complex-grafted polymers **Poly(NVK-*co*-[Ir(iqbt)$_2$(vb-ppy)])** and **Poly(vinyl-PBD)-*co*-NVK-*co*-[Ir(iqbt)$_2$(vb-ppy)])**

layer (ETL) towards the facilitated carriers' balance for some multi-layer NIR-PLEDs,[12] the issues of device instability and undesirable efficiency-roll-off caused by the heterogeneity of the Ir(III)-complex-doping polymer systems are still difficult to be addressed.

To circumvent such problems, to some extent, we can rely on a conceptual approach to use Ir(III)-complex-grafted polymers towards their solution-processed multi-layer NIR-PLEDs. On one hand, benefiting from the covalent-bonding linkage, the NIR-emitting Ir(III)-complexes are molecularly dispersed into a hole-transporting polymer host with a uniform phase. Meanwhile, further through the doping or grafting of the electron-transport molecule, the resultant Ir(III)-complex-grafted polymers could be indicative of a bipolar (electron/hole-transport ability) nature. Especially through the smooth feeding ratio tunings of both Ir(III)-complex and electron-transport molecule into the hole-transport polymer matrix, it can provide a big room to facilely reform the carrier's balance within the bipolar polymer towards an optimized optoelectronic feature. Noticeably, although bipolar Ir(III)-complex-grafted polymers capable of showing monochromatic[13] or panchromatic[14] emission in the visible-light range are achieved, no examples of their fabrications for NIR-PLEDs, to our knowledge, are reported. Herein, taking the NIR-emitting **[Ir(iqbt)$_2$(vb-ppy)]** with one vinyl group as the polymerizable complex monomer, as shown in **Scheme 1**, two series of Ir(III)-complex-grafted polymers **Poly(NVK-*co*-[Ir(iqbt)$_2$(vb-ppy)])** (100:1, 150:1 or 200:1) and **Poly((vinyl-PBD)-*co*-NVK-*co*-[Ir(iqbt)$_2$(vb-ppy)])** (15:150:1) are obtained from its copolymerization with NVK and/or monomer **vinyl-PBD** with the facilitated electron-transport, respectively. Moreover, using the Ir(III)-complex-grafted polymer doped or grafted with electron-transport molecule as the EML, respectively, the first-examples of bipolar Ir(III)-complex-grafted NIR-PLEDs are also pursued.

2. Experimental section

The information on starting materials and general characterization methods has been provided in the Electronic Supporting Information (ESI). The HC^N[1] main ligand **Hiqbt** was synthesized by the Suzuki coupling of 2-Cl-isoquinoline with benzo[b]thien-2-yl boronic acid as reported in our recent literature.[8(e)] As to the μ-chloro-bridged dimeric intermediate **[Ir(iqbt)$_2$(μ-Cl)]$_2$**, it was prepared according to the typical Nonoyama procedure.[15] For the vinyl-functionalized HC^N[2] ancillary ligand **vb-Hppy**, it was synthesized from the improved Suzuki coupling reaction of 4-vinylphenyl-boronic acid with 2-(4-bromophenyl)-pyridine as in the literature.[16] The vinyl-modified electron-transport monomer **vinyl-PBD** was obtained through the dehydration cyclization[17] and the subsequent Suzuki coupling reaction.[18]

Synthesis of the vinyl-functionalized complex monomer [Ir(iqbt)$_2$(vb-ppy)]

To a solution of the μ-chloro-bridged dimeric intermediate **[Ir(iqbt)$_2$(μ-Cl)]$_2$** (270 mg, 0.18 mmol) in mixed solvents of CH_2Cl_2 (8 mL) and MeOH (4 mL), the synthesized **vb-Hppy** (139 mg, 0.54 mmol) and $AgCF_3SO_3$ (138 mg, 0.54 mmol) were added, and the mixture was heated at 45 °C under a dry N_2 atmosphere for 24 h. After cooling to room temperature, the white solid was removed and the residual was purified by column chromatography on silica gel using CH_2Cl_2/acetonitrile (v/v = 2:1) as the eluent. Yield: 35 mg (20%). Calc. for $C_{53}H_{34}IrN_3S_2$: C, 65.68; H, 3.54; N, 4.34%. Found: C, 65.63; H, 3.58; N, 4.30%. FT-IR (KBr, cm^{-1}): 3051 (w), 2953 (m), 2918 (m), 2851 (m), 2359 (w), 1618 (w), 1601 (w), 1582 (w), 1558 (w), 1541 (w), 1501 (w), 1468 (w), 1452 (w), 1435 (m), 1412 (s), 1375 (w), 1360 (w), 1335 (m), 1306 (w), 1288 (w), 1273 (w), 1231 (m), 1157 (w), 1148 (w), 1124 (w), 1067 (w), 1040 (w), 1020 (w), 988 (w), 962 (w), 910 (m), 862 (w), 845 (w), 806 (m), 779 (w), 760 (m), 727 (vs), 706 (w), 687 (s), 662 (m), 633 (w), 598 (w), 565 (w), 528 (w), 500 (w). ^{1}H NMR (400 MHz, $CDCl_3$): δ (ppm) 9.27 (d, 1H, -Py), 8.80 (d, 1H, -Py), 8.51 (d, 1H, -Py), 8.06 (d, 1H, -Py), 8.02 (d, 1H, -Py), 7.95 (m, 7H, -Ph), 7.84 (t, 2H, -Ph), 7.69 (t, 2H, -Ph), 7.64 (d, 1H, -Py), 7.61 (d, 2H, -Ph), 7.58 (d, 1H, -Py), 7.53 (t, 2H, -Ph), 7.49 (d, 1H, -Ph), 7.39 (d, 1H, -Ph), 7.23 (d, 1H, -Ph), 7.17 (m, 2H, -Ph), 7.11 (t, 1H, -Ph), 6.88 (t, 2H, -Ph), 6.82 (t, 1H, -Ph), 6.66 (t, 1H, -CH=), 5.65 (d, 1H, =CH_2), 5.15 (d,1H, =CH_2). ESI-MS (in CH_2Cl_2) *m/z*: 970.21 (100%), $[M+H]^+$.

Synthesis of the Ir^{3+}-complex-grafted polymers Poly(NVK-*co*-[Ir(iqbt)$_2$(vb-ppy)]) (100:1, 150:1 or 200:1)

A mixture of NVK and the complex monomer **[Ir(iqbt)$_2$(vb-ppy)]** at a stipulated feed molar ratio (100:1, 150:1 or 200:1) in the presence of AIBN (azobis(isobutyronitrile); 1.5 mol% of NVK) was dissolved in toluene (30 mL), and the resultant homogeneous solution was purged with N_2 for 10 min and sealed under a reduced N_2

atmosphere. The reaction mixture was heated to 80 °C with continuous stirring for 48 h. The viscous mixture was diluted with toluene (15 mL) and precipitated with *n*-hexane (50 mL) for three times. The resulting solid products were collected by filtration and dried at 45 °C under vacuum to constant weight, respectively. For the **Poly(NVK-*co*-Ir(iqbt)$_2$(vb-ppy))** (150:1): Yield: 92%. FT-IR (KBr, cm^{-1}): 3059 (w), 2968 (w), 2934 (w), 2359 (w), 1597 (w), 1483 (m), 1450 (s), 1325 (m), 1223 (m), 1157 (w), 1124 (w), 1028 (w),1003 (w), 926 (w), 829 (w), 745 (vs), 721 (s), 617 (w), 567 (w), 528 (w).^{1}H NMR (400 MHz, $CDCl_3$): δ (ppm) 9.24 (m, 3H, -Ph), 8.10-6.04 (br, 1100H+26H), 5.52-2.75 (br, 138H), 2.38 (b, 1H), 1.65 (b, 2H), 1.30-0.88 (b, 276H). XPS result: 0.80 mol% *versus* NVK. The characterization of the other Ir^{3+}-complex-grafted polymers **Poly(NVK-*co*-[Ir(iqbt)$_2$(vb-ppy)])** (100:1 or 200:1) was provided in the ESI.

Synthesis of the bipolar Ir^{3+}-polymer Poly((vinyl-PBD)-*co*-NVK-*co*-[Ir(iqbt)$_2$(vb-ppy)]) (15:150:1)

The bipolar Ir^{3+}-polymer **Poly((vinyl-PBD)-*co*-NVK-*co*-[Ir(iqbt)$_2$(vb-ppy)])** (15:150:1) was synthesized in the same way as the **Poly(NVK-*co*-[Ir(iqbt)$_2$(vb-ppy)])** (150:1) except that the mixture of the organic monomer **vinyl-PBD**, NVK and the complex monomer **[Ir(iqbt)$_2$(vb-ppy)]** at a stipulated feed molar ratio of 15:150:1 (1.5 mol% of AIBN relative to NVK) instead of the mixture of NVK and the complex monomer **[Ir(iqbt)$_2$(vb-ppy)]** at a feeding ratio of 150:1 (1.5 mol% of AIBN relative to NVK) was adopted. For the **Poly((vinyl-PBD)-*co*-NVK-*co*-[Ir(iqbt)$_2$(vb-ppy)])** (15:150:1): Yield: 91%. FT-IR (KBr, cm^{-1}): 3051 (w), 2963 (w), 2932 (w), 2354 (w), 1598 (w), 1483 (m), 1452 (s), 1333 (m), 1225 (m), 1157 (w), 1124 (w), 1027 (w),1003 (w), 924 (w), 829 (w), 742 (vs), 723 (s), 616 (w), 568 (w), 529 (w).^{1}H NMR (400 MHz, $CDCl_3$): δ (ppm) 8.13-5.93 (br, 1135H), 4.92-2.39 (b, 135H), 1.59 (s, 135H), 1.28-0.91 (b, 270H). XPS result: 0.78 mol% *versus* NVK.

Device designs of the doping-type NIR-PLED-I based on the Ir^{3+}-complex monomer and the grafting-type NIR-PLEDs-II-III based on the Ir^{3+}-polymers

Using a mixture of the complex monomer **[Ir(iqbt)$_2$(vb-ppy)]** (5 wt%) and the *co*-host PVK:PBD (65:30, wt%; PVK = Poly(*N*-vinyl-carbazole), PBD = (2-(4-*tert*-butylphenyl)-5-(4-biphenylyl)-1,3,4-oxadiazole)) as the EML, the doping-type **NIR-PLED-I** was fabricated with the configuration of ITO/PEDOT:PSS (40 nm)/PVK:PBD:**[Ir(iqbt)$_2$(vb-ppy)]** (120 nm)/TmPyPB (15 nm)/LiF (1 nm)/Al (100 nm) for comparison. As to the grafting-type **NIR-PLEDs-II-III**, they were fabricated with the configurations of ITO/PEDOT:PSS (40 nm)/**Poly(NVK-*co*-[Ir(iqbt)$_2$(vb-ppy)])** (150:1):PBD (30 wt%) (120 nm)/TmPyPB (15 nm)/LiF (1 nm)/Al (100 nm) and ITO/PEDOT:PSS (40 nm)/**Poly((vinyl-PBD)-*co*-NVK-*co*-[Ir(iqbt)$_2$(vinyl-ppy)])** (15:150:1) (120 nm)/TmPyPB (15 nm)/LiF (1 nm)/Al (100 nm), respectively. Their difference lies in the usage of PVK:PBD:**[Ir(iqbt)$_2$(vb-ppy)]** for the **NIR-PLED-I**, **Poly(NVK-*co*-[Ir(iqbt)$_2$(vb-ppy)])** (150:1):PBD for the **NIR-PLED-II** or **Poly((vinyl-PBD)-*co*-NVK-*co*-[Ir(iqbt)$_2$(vb-ppy)])** (15:150:1) for the **NIR-PLED-III**, respectively. TmPyPB (1,3,5-tri[(3-pyridyl)-phen-3-yl]benzene) was used to further promote electron-transport ability in the **NIR-PLEDs-I-III**. Details of the series of NIR-PLEDs fabrication and their testing are presented in the ESI.

3. Results and discussion

Synthesis, characterization and photo-physical property of the Ir^{3+}-complex monomer [Ir(iqbt)$_2$(vb-ppy)]

Through the improved Suzuki coupling reaction[8(e)] of 2-Cl-isoquinoline (instead of 2-Br-isoquinoline[7(g)]) with benzo[*b*]thien-2-yl boronic acid, the synthesized HC^N^1 main ligand **Hiqbt** was cyclometalated with $IrCl_3.nH_2O$ to give the μ-chloro-bridged dimeric intermediate **[Ir(iqbt)$_2$(μ-Cl)]$_2$** as the literature.[15] Also as shown in **Scheme 1**, further based on the cyclometalation of the intermediate **[Ir(iqbt)$_2$(μ-Cl)]$_2$** with another vinyl-functionalized HC^N^2 ancillary **vb-Hppy** by $AgCF_3SO_3$ to the chloride-free, the vinyl-functionalized [Ir(C^N^1)$_2$(C^N^2)] complex monomer **[Ir(iqbt)$_2$(vb-ppy)]** was obtained.

The vinyl-functionalized complex monomer **[Ir(iqbt)$_2$(vb-ppy)]** was well characterized *via* EA, FT-IR, ^{1}H NMR and ESI-MS, despite the failure of its single-crystals. Evidently, in the ^{1}H NMR spectrum (**Figure S1**) of the complex monomer **[Ir(iqbt)$_2$(vb-ppy)**, the stipulated molar ratio of 2:1 between the C^N^1 (**iqbt**)$^-$ and the C^N^2 (**vb-ppy**)$^-$ proton resonances confirms its desirable [Ir(C^N^1)$_2$(C^N^2)] component. Meanwhile, contributing from the incorporation of the asymmetric vinyl-functionalized HC^N^2 ancillary **vb-Hppy**, the point group of its complex monomer **[Ir(iqbt)$_2$(vb-ppy)]** is C_1, from which the two sets of doublet peaks at δ = 8.80 and 8.51 ppm can be safely assigned to the two protons on the C atoms adjacent to N atoms in the pyridyl rings of the two (**iqbt**)$^-$-C^N^1 ligands, respectively. Moreover, upon the Ir(III)-coordination, besides the double signal (δ = 9.27 ppm) of the proton on the C atom adjacent to N atoms in the pyridyl ring of the (**vb-ppy**)$^-$-C^N^2 ligand being significantly down-field shifted to that (δ = 8.70 ppm) for the free **vb-Hppy**, the slightly high-field shifts (δ = 6.66, 5.65 and 5.15 ppm) of the vinyl-terminal proton resonances for the complex monomer **[Ir(iqbt)$_2$(vb-ppy)]** relative to those (δ = 6.78, 5.82 and 5.30 ppm) of the free **vb-Hppy**, further verifies the successful vinyl-modification. Furthermore, the ESI-MS result of the complex monomer **[Ir(iqbt)$_2$(vb-ppy)]** exhibits the strongest mass peak at *m/z* 970.21 assigned to the major species [M+H]$^+$, indicating that its [Ir(C^N^1)$_2$(C^N^2)]-characteristic unit can remain stable in solution.

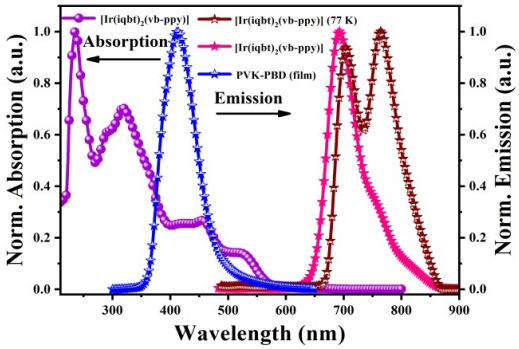

Figure 2. Normalized UV-Visible-NIR absorption and emission spectra for **[Ir(iqbt)$_2$(vb-ppy)]** (λ_{ex} = 463 nm) in degassed CH_2Cl_2 solution and PVK-PBD (65:30, weight ratio; λ_{ex} = 273 nm) in film at RT or 77 K.

The photo-physical properties of the complex monomer **[Ir(iqbt)$_2$(vb-ppy)]** were examined in degassed solution at RT or 77 K, and the results are summarized in **Table S2** and **Figure 2**. As shown in **Figure 2**, in contrast to the limited (λ_{ab} < 400 nm; **Figure S2**) absorptions of the two kinds of C^N ligands, the complex monomer **[Ir(iqbt)$_2$(vb-ppy)]** exhibits the significantly broadened UV-visible-NIR absorption: the intense absorption bands below 420 nm from the intraligand π-π* transitions, the moderate absorption bands (λ_{ab} = 456, 487 (sh), 518 and 557 (sh) nm) assigned to the ^{1,3}LLCT/^{1,3}MLCT-admixed (LLCT = ligand-to-ligand charge transfer; MLCT = metal-to-ligand charge transfer) transitions, and the weak bands extending over 600 nm probably from the $S_0 \rightarrow T_1$ excitation. Upon photo-excitation at λ_{ex} = 463 nm, the complex monomer **[Ir(iqbt)$_2$(vb-ppy)]** displays the strong NIR emission (58% of the $\lambda_{em} \geq$ 700 nm proportion) peaking at 693 nm with a shoulder at 754 nm (**Figure 2**). In contrast to the non-emissive character (λ_{em} = 415 nm for the HC^N^1 ligand **Hiqbt** and λ_{em} = 403 nm for the HC^N^2 ligand **vb-Hppy**; **Figure S2**) of the two C^N ligands in the NIR range, the NIR emission of the complex monomer **[Ir(iqbt)$_2$(vb-ppy)]** should originate from the Ir^{3+}-induced T_1 state. Moreover, the time-decayed mono-exponential lifetime of 0.25 μs (**Figure S3**) was obtained at λ_{em} = 693 nm for the complex monomer **[Ir(iqbt)$_2$(vb-ppy)]** species, confirming the intrinsic NIR-phosphorescent nature. Noticeably, the NIR-emissive lifetime (= τ0.25μ s) is remarkably shorter than those of the heteroleptic Ir^{3+}-complexes [Ir(iqbt)$_2$(O^O)][7(d), 7(g)] or [Ir(iqbt)$_2$(N^O)],[8(e)] which should be originated from the stronger π-backbonding effect[19] due to the asymmetric C^N^2-(**vb-ppy**) ancillary π-donor in the complex monomer **[Ir(iqbt)$_2$(vb-ppy)]** with a restricted vibronic motion to the NIR-emitting excited-state. Accordingly, owing to the large radiative rate constant (k_r = 7.6 × 10^5 s^{-1}), its NIR-emissive efficiency of Φ_{PL} = 0.19 is realized. Furthermore, as illustrated for the emission (85% of the $\lambda_{em} \geq$ 700 nm proportion; **Figure 2**) with a well-resolved vibronic structure at 77 K, the 0-0 transition at 704 nm and the 0-1 transition at 764 nm with small bathochromatic shifts compared to the RT one (**Figure 2**), give a Huang-Rhys factor (S_M) of 0.98, suggesting that the complex monomer **[Ir(iqbt)$_2$(vb-ppy)]** has a weak geometry distortion[20] of the T_1 state relative to the ground state. As a result, the thermal gravimetric (TG; **Figure S4**) analysis reveals that the complex monomer **[Ir(iqbt)$_2$(vb-ppy)]** exhibits a desirably good thermal stability with the comparable decomposition temperature (T_d, with 5 wt% weight loss) of 384 °C to those of typical [Ir(C^N)$_3$]-homoleptic[6] complexes.

Electronic structure calculations of the complex monomer [Ir(iqbt)$_2$(vb-ppy)]

To explore the absorption nature of the complex monomer **[Ir(iqbt)$_2$(vb-ppy)]**, DFT/TD-DFT (time-dependent density functional theory) calculations based on its optimized S_0 geometry were performed, and the results are summarized in **Table S3** and **Figure 3**. As shown in **Figure 3**, in contrast to the almost entire contribution (92.76%) from one C^N^1-(**iqbt**)$^-$ main ligand to the LUMO, the HOMO is mainly (51.01% and 23.06%) localized at the two C^N^1-(**iqbt**)$^-$ main ligands and accompanied by the substantial (23.73%) contribution from the Ir(III)-centre and the less (2.20%) contribution from the C^N^2-(**vb-ppy**)$^-$ ancillary ligand. However, different from the dominated (84.71%) contribution from one C^N^1-(**iqbt**)$^-$ main ligand and the more substantial (10.22%) contribution from the C^N^2-(**vb-ppy**)$^-$ ancillary ligand to the LUMO+1, the LUMO+2 is predominantly (86.93%) located at the C^N^2-(**vb-ppy**)$^-$ ancillary ligand. Meanwhile, besides the prevalent (74.44%) contribution

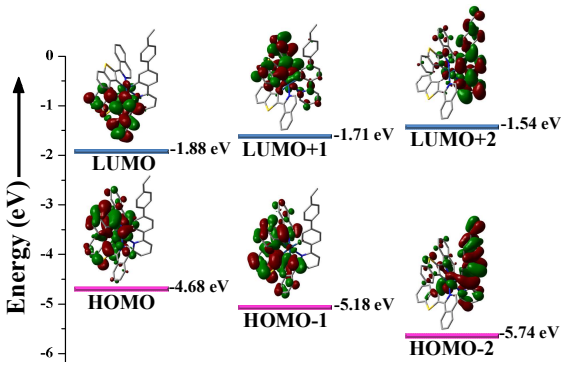

Figure 3. The HOMO and LUMO patterns for the complex monomer **[Ir(iqbt)$_2$(vb-ppy)]** based on its optimized S_0 geometry.

from the two C^N^1-(**iqbt**)$^-$ main ligands to the HOMO-2 like the HOMO-1 (97.79%), some substantial contributions from the Ir(III)-centre (14.59%) and the C^N^2-(**vb-ppy**)$^-$ ancillary ligand (10.97%) are observed. Further checking from **Table S3**, the calculated $S_0 \rightarrow S_n$ (n = 1-4) transition absorption wavelengths of the complex monomer **[Ir(iqbt)$_2$(vb-ppy)]** are predicted at 558, 512, 489 and 445 nm, respectively. For the $S_0 \rightarrow S_1$ transition absorption at 558 nm, the population analysis of the HOMO → LUMO (97.64%) transition verifies the partial (22.7%) ^{1}MLCT, the substantial (21.6%) ^{1}ILCT (intraligand charge transfer) and the dominated (51.4%) ^{1}LLCT feature from the π orbitals of one C^N^1-(**iqbt**)$^-$ main ligand to the π* orbitals of the other one. The calculated absorption peak at 512 nm, 489 nm or 445 nm mainly results from the corresponding HOMO → LUMO+1 (95.32%), HOMO → LUMO+2 (97.26%) or HOMO-1 → LUMO (76.73%) transition, respectively, also exhibiting the ^{1}LLCT/^{1}MLCT-admixed character. Hence, all the calculated absorptions featured with ^{1}LLCT/^{1}MLCT-admixed transitions are in good agreement with the experimental data (λ_{ab} = 557, 518, 487 and 456 nm) of the complex monomer **[Ir(iqbt)$_2$(vb-ppy)]** in solution. Interestingly, due to the large contribution combined from the HOMO → LUMO (59.94%) and the HOMO-1 → LUMO (30.32%) transitions to the T_1 state, the experimental $S_0 \rightarrow T_1$ absorption (over 600 nm) transition can be reasonably assigned to the ^{3}ILCT/^{3}MLCT/^{3}LLCT-admixed transitions.

In order to definitely elucidate its NIR-emissive behaviour of the complex monomer **[Ir(iqbt)$_2$(vb-ppy)]**, natural transition orbital (NTO; T**able S4** and **Figure 4**) calculations were further performed on its optimized T_1 geometry, where based on the entire (100%) Hole → Particle transition, the ^{3}ILCT dominated (73.8%) and the less

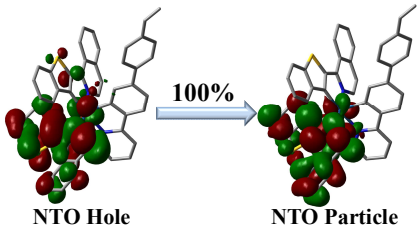

Figure 4. The NTO pattern for the $T_1 \rightarrow S_0$ emission of the complex monomer **[Ir(iqbt)$_2$(vb-ppy)]** based on its optimized T_1 geometry.

prevalent (13.9%) ^{3}MLCT transitions are responsible for its NIR-emitting phosphorescence.

Synthesis, characterization and photo-physical properties of the two series of Ir^{3+}-complex-grafted polymers

Considering the excellent physical properties (high thermal stability, good mechanical intensity and excellent spin-coated film-formability, etc.) of the *semi*-conducting PVK as a popular polymer host,[21] the grafting-type Ir^{3+}-polymers **Poly(NVK-*co*-[Ir(iqbt)$_2$(vb-ppy)])** with different feeding ratios (100:1, 150:1 or 200:1) were synthesized from the AIBN-initiated copolymerization (**Scheme 1**) of NVK and the complex monomer **[Ir(iqbt)$_2$(vb-ppy)]**. As a matter of fact, not only does the PVK host function as hole-transport matrix, it with the significantly higher T_1 level also acts as an effective energy donor to transfer energy *via* Förster mechanism[22] to the low energy-state Ir^{3+}-complex-acceptor. Moreover, to further overcome the electron-transport deficiency of the Ir^{3+}-polymers **Poly(NVK-*co*-[Ir(iqbt)$_2$(vb-ppy)])**, another grafting-type Ir^{3+}-polymer **Poly((vinyl-PBD)-*co*-NVK-*co*-[Ir(iqbt)$_2$(vb-ppy)])** (also **Scheme 1**) was designed, where through the AIBN-assisted ternary copolymerization of NVK, the complex monomer **[Ir(iqbt)$_2$(vb-ppy)]** and the electron-transport monomer **vinyl-PBD**, the bipolar (electron/hole-transport) Ir^{3+}-polymer **Poly((vinyl-PBD)-*co*-NVK-*co*-[Ir(iqbt)$_2$(vb-ppy)])** (15:150:1) was obtained.

To verify the AIBN-assisted radical copolymerization,[23] all the two series of grafting-type Ir^{3+}-polymers were characterized by FT-IR, ^{1}H NMR and GPC (gel permeation chromatography) methods. On one hand, in the ^{1}H NMR spectrum (**Figure S1**) of the representative **Poly(NVK-*co*-[Ir(iqbt)$_2$(vb-ppy)])** (150:1) or **Poly((vinyl-PBD)-*co*-NVK-*co*-[Ir(iqbt)$_2$(vb-ppy)])** (15:150:1), the presence of the broadened proton resonances of the polymerized **[Ir(iqbt)$_2$(vb-ppy)]**, NVK and/or **vinyl-PBD**, together with the disappearance of their original vinyl-characteristic proton resonances, indicate that the complex monomer **[Ir(iqbt)$_2$(vb-ppy)]** and/or the **vinyl-PBD** are actually covalent-bonded into the corresponding PVK backbone. On the other hand, GPC results (**Table S5**) show that all the PDIs (PDI = M_w/M_n) with different feed molar ratios for the two kinds of the grafting-type Ir^{3+}-polymers are in the relatively narrow range (< 1.30) due to the AIBN-initiated radical copolymerization.[23] Moreover, with regard to the actual Ir^{3+}-complex-grafting content, the XPS (x-ray photoelectron spectroscopy) quantitative analyses reveal that every Ir^{3+}-complex-grafting content is found to be slightly higher than the correspondingly initial feeding ratio, which probably arises from the loss of oligomeric PVK during the isolation of one specific Ir^{3+}-polymer.[24] Furthermore, the PXRD (powder X-ray diffraction) pattern (**Figure S5**) of either the **Poly(NVK-*co*-[Ir(iqbt)$_2$(vb-ppy)])** or the **Poly((vinyl-PBD)-*co*-NVK-*co*-[Ir(iqbt)$_2$(vb-ppy)])** just exhibits the PVK-based amorphous peaks, suggesting the low-concentration homogeneous dispersion of the monomers **[Ir(iqbt)$_2$(vb-ppy)]** and/or **vinyl-PBD** into the PVK backbone. TG and DSC (differential scanning calorimetric; **Figure S4**) results of these grafting-type Ir^{3+}-polymers show that the improved (T_d; > 400 °C) thermal stability over that (384 °C) of the complex monomer **[Ir(iqbt)$_2$(vb-ppy)]**, and the desirable T_g (glass transition temperature) above 160 °C are observed.

The photo-physical properties of the two series of grafting-type Ir^{3+}-polymers **Poly(NVK-*co*-[Ir(iqbt)$_2$(vb-ppy)])** (100:1, 150:1 or 200:1) and **Poly((vinyl-PBD)-*co*-NVK-*co*-[Ir(iqbt)$_2$(vb-ppy)])** (15:150:1) were investigated in solid-state or solution at RT, and the data are summarized in **Table S2** and **Figures 5 and S6**. As shown in **Figure S6**, both the DR (diffuse reflection) and the solution

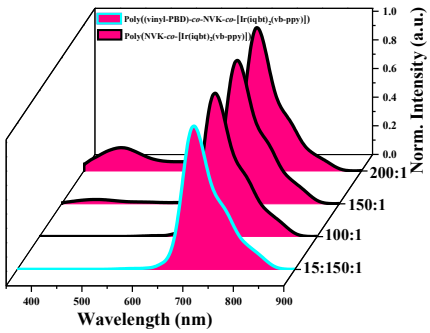

Figure 5. Normalized emission spectra of the Ir^{3+}-polymers **Poly(NVK-*co*-[Ir(iqbt)$_2$(vb-ppy)])** (100:1, 150:1 or 200:1) and **Poly((vinyl-PBD)-*co*-NVK-*co*-[Ir(iqbt)$_2$(vb-ppy)])** (15:150:1) in solid-state at RT.

absorption spectra of all the grafting-type Ir^{3+}-polymers show the significantly broader absorption bands than that of the PVK, in which, besides the strong absorptions below 400 nm attributed to the π-π* transitions from the organic portions of PVK and the ligands, the absorptions across the whole visible range should be assigned to the ^{1,3}LC/^{1,3}MLCT and $S_0 \rightarrow T_1$ admixed transitions of the grafted complex monomer **[Ir(iqbt)$_2$(vb-ppy)]**. Noticeably, owing to the significant spectral overlap (also **Figure 2**) between the absorption of the complex monomer **[Ir(iqbt)$_2$(vb-ppy)]** and the emission of PVK, effective Förster energy transfer[22] should be motivated. Convincingly, upon photo-excitation, the resulting emissions (**Figure 4**) of all the grafting-type Ir^{3+}-polymers do not show the simple addition spectra, but they are highly enslaved to the stipulated feeding ratio. For the **Poly(NVK-*co*-[Ir(iqbt)$_2$(vb-ppy)])** (100:1 or 150:1), photo-excitation gives rise to the almost entire NIR emission (λ_{em} = 696 nm), resembling that (**Figure 2**) of the complex monomer **[Ir(iqbt)$_2$(vb-ppy)]** in solution. The absence of the PVK-based blue-light is due to the effective Förster energy transfer[22] from the PVK to the Ir^{3+}-complex-acceptor, giving rise to the satisfactory Φ_{PL} of 0.13 (100:1) or 0.16 (150:1). Further increasing the feeding ratio up to 200:1, the dual-emitting (Φ_{PL} = 0.21) behaviour associated with the PVK-centered emission at 420 nm and the Ir^{3+}-complex-based NIR emission (λ_{em} = 690 nm), is observed, and the 28 ns of the PVK-centered lifetime together with the Ir^{3+}-complex-decayed lifetime of 1.29 μs further confirm the dual-emitting character (**Figure S7**). Accordingly, based on the equation[25] of Φ_{ET} = 1-(τ_{DA}/τ_D) (τ_{DA} or τ_D is the donor's amplitude-weighted lifetime with and without acceptor, respectively; τ_D = 44 ns (λ_{em} = 430 nm) for the pure PVK as in the literature[26]) for the **Poly(NVK-*co*-[Ir(iqbt)$_2$(vb-ppy)])** (200:1), the Förster energy transfer Φ_{ET} of 36% is qualitatively estimated. For comparison, accompanying with the almost constant and mono-exponential Ir^{3+}-complex-decayed lifetime (1.24 μs) for the **Poly(NVK-*co*-[Ir(iqbt)$_2$(vb-ppy)])** (150:1) while the significantly reduced lifetime of 0.97 μs for the **Poly(NVK-*co*-[Ir(iqbt)$_2$(vb-ppy)])** (100:1), the facilitated separation of the complex monomers **[Ir(iqbt)$_2$(vb-ppy)]** within the PVK backbone should occur at the lower Ir^{3+}-complex-grafting level (150:1 or 200:1), from which, the undesirable aggregation-caused quenching (ACQ)[27] effect from the high grafting content (100:1) is effectively suppressed. Interestingly, with an appropriate amount of the electron-transport **vinyl-PBD** further grafted for the bipolar **Poly((vinyl-PBD)-*co*-NVK-*co*-[Ir(iqbt)$_2$(vb-ppy)])** (15:150:1), besides the similar Ir^{3+}-complex-based NIR emission (λ_{em} = 693 nm) to that of the **Poly(NVK-*co*-[Ir(iqbt)$_2$(vb-**

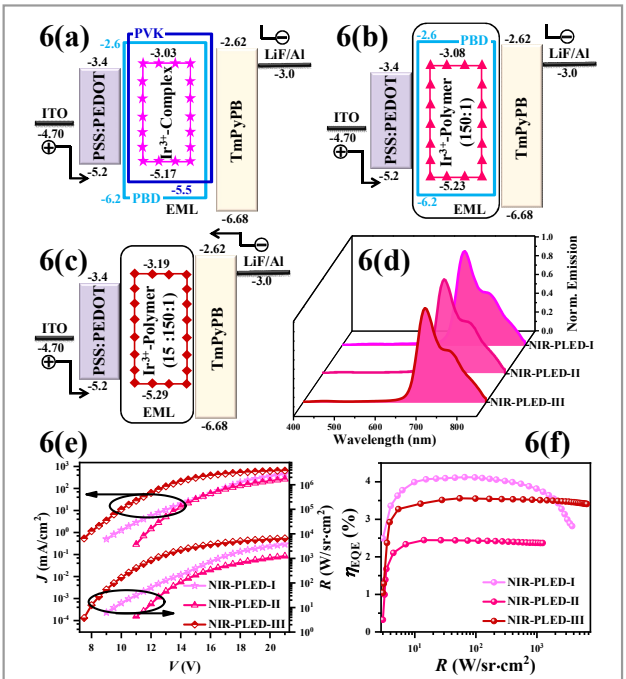

Figure 6. Device structures and energy level diagrams for the doping-type **NIR-PLED-I** (a) and the grafting-type **NIR-PLEDs-II-III** (b-c); Normalized EL spectra (d); *R-J-V* (e) and η_{EQE}-*R* curves (f).

ppy)]) (150:1), its typical and comparable NIR-emitting phosphorescence (τ = 1.25 μs and Φ_{PL} = 0.17) is also observed.

Device performance of NIR-PLEDs-I-III based on the complex monomer [Ir(iqbt)$_2$(vb-ppy)] and its Ir^{3+}-polymers

Thanks to the suitability of PVK-PBD (65:30; wt%) with good hole/electron transports as the *co*-host,[28] it is of interest on using the efficient NIR-emitting complex monomer **[Ir(iqbt)$_2$(vb-ppy)]** as the dopant (5 wt%) for the prototype **NIR-PLED-I** with a configuration shown in **Figure 6(a)**. Attributing to the experimental (**Figure S8**) HOMO (-5.17 eV) and LUMO (-3.03 eV) levels of the complex monomer **[Ir(iqbt)$_2$(vb-ppy)]** aligned well within the band gap (-6.2~-5.5 eV of HOMO and -2.6~-2.0 eV of LUMO) of PVK-PBD, the injected electrons and holes through the PVK-PBD matrix are firstly trapped, and then direct charge trapping[29] should occur within the NIR-emitting Ir(III)-complexes. As expected, as shown in **Figure 6(d)**, the electroluminescent spectra of the **NIR-PLED-I** are voltage-independent while just Ir(III)-complex-related NIR (λ_{em} = 696 and 756 (sh) nm; ca. 70% of the $\lambda_{em} \geq$ 700 nm proportion) emissions well resembled that (also **Figure 2**) of the complex monomer **[Ir(iqbt)$_2$(vb-ppy)]** in solution. The absence of the PVK-PBD residual light indicates that the effective Förster energy transfer[22] also takes place within the doping EML upon electrical driving. For the **NIR-PLED-I**, upon the turn-on voltage (V_{on}, defined as the voltage of the output irradiance (*R*) = 5.0 W/sr·cm^2) of 9.0 V, as shown in **Figure 6(e)**, both the *R* and the current density (*J*) monotonically increase with the increase of the applied bias voltage (*V*), exhibiting the R^{Max} of 3772.1 W/sr·cm^2 with the J^{max} of 452.8 mA/cm^2 at 21.0 V. Meanwhile, the **NIR-PLED-I** exhibits the *R*-regulated waving for the η_{EQE} (**Figure 6(f)**), where the η_{EQE}^{Max} of 4.1% with the *R* = 65.5 W/sr·cm^2 at 12.0 V and about 30% efficiency-roll-off in the higher radiance range of *R* = 65.5-3772.1 W/sr·cm^2 are observed. Worthy of note, contributing from more excitons confined within the broadened recombination zone supplemented with the facilitated electron-transport TmPyPB,[30] the overall device performance of the **NIR-PLED-I**, is at the top-level (also **Figure 1**) and comparable to the best one[7(c)] among the previously reported NIR-PLEDs.

Considering the almost identical Ir^{3+}-complex-grafted content between **Poly(NVK-*co*-[Ir(iqbt)$_2$(vb-ppy)])** (150:1) and **Poly((vinyl-PBD)-*co*-NVK-*co*-[Ir(iqbt)$_2$(vb-ppy)])** (15:150:1) comparable to that of the doping system (PVK:PBD:**[Ir(iqbt)$_2$(vb-ppy)]**; 65:30:5, wt%) for the **NIR-PLED-I**, the bipolar Ir^{3+}-polymers of **Poly(NVK-*co*-[Ir(iqbt)$_2$(vb-ppy)])** (150:1) and **Poly((vinyl-PBD)-*co*-NVK-*co*-[Ir(iqbt)$_2$(vb-ppy)])** (15:150:1) further doped with PBD and grafted with **vinyl-PBD** were used as the EML for the grafting **NIR-PLEDs-II-III** (**Figures 6(b-c)**), respectively. Through the further grafting of the **vinyl-PBD** for the **Poly((vinyl-PBD)-*co*-NVK-*co*-[Ir(iqbt)$_2$(vb-ppy)])** (15:150:1), the electron-transport promotion is reflected from its experimentally (**Figure S9**) stabilized LUMO level (-3.19 eV) in comparison to that (-3.08 eV) of the **Poly(NVK-*co*-[Ir(iqbt)$_2$(vb-ppy)])** (150:1). Excitingly, for both the **NIR-PLED-II** with the doping of PBD into the **Poly(NVK-*co*-[Ir(iqbt)$_2$(vb-ppy)])** (150:1) and the **NIR-PLED-III** based on the **Poly((vinyl-PBD)-*co*-NVK-*co*-[Ir(iqbt)$_2$(vb-ppy)])** (15:150:1), the Ir(III)-complex-exclusive NIR-emissive spectra similar to those of the **NIR-PLED-I** or their photo-luminescent results (also **Figure 5**) in solid-states are observed. As compared with the **NIR-PLED-I**, due to the deeper LUMO gap between PBD and the **Poly(NVK-*co*-[Ir(iqbt)$_2$(vb-ppy)])** (150:1), the V_{on} of the **NIR-PLED-II** is up to 11.0 V. Moreover, the decreased η_{EQE}^{max} of 2.5% and the R^{Max} of 1239.2 W/sr·cm^2 show a good trade off with the significantly alleviated (ca. 3%) efficiency roll-off within the 12.0-21.0 range, which should be attributed to the less carrier-trapping probability with the better carrier-balance within the **Poly(NVK-*co*-[Ir(iqbt)$_2$(vb-ppy)])** (150:1). By contrast, using the **Poly((vinyl-PBD)-*co*-NVK-*co*-[Ir(iqbt)$_2$(vb-ppy)])** (15:150:1) as the bipolar EML for the **NIR-PLED-III**, Förster energy transfer[22] and carrier-trapping[29] mechanisms also concurrently proceed within the TmPyPB-assisted recombination zone.[30] Interestingly, for the **NIR-PLED-III**, besides the low V_{on} at 7.5 V and the η_{QE}^{max} up to 3.6% at 9.0 V, the high R^{Max} of 6559.3 W/sr·cm^2 at 21.0 V is at the cost of the highest J^{max} of 647.5 mA/cm^2. Nonetheless, the superior device performance of the **NIR-PLED-III** is represented by the η_{QE}^{max} of 3.6% (9.0 V) and the weak (ca. 4%) efficiency roll-off with a preserved η_{QE} of 3.4% at 21.0 V, which means that the high-efficiency of the **NIR-PLED-I** and the negligible efficiency roll-off of the **NIR-PLED-II** are well realized for the **NIR-PLED-III**. Importantly, this result engenders bipolar Ir(III)-complex-grafted polymers a conceptual strategy to high-performance NIR-PLEDs.

4. Conclusions

In summary, through the copolymerization of NVK, the vinyl-functionalized NIR-emitting monomer **[Ir(iqbt)$_2$(vb-ppy)]** and/or the electron-transporting monomer **vinyl-PBD**, two series of Ir(III)-complex-grafted polymers **Poly(NVK-*co*-[Ir(iqbt)$_2$(vb-ppy)])** (100:1, 150:1 or 200:1) and **Poly((vinyl-PBD)-*co*-NVK-*co*-[Ir(iqbt)$_2$(vb-ppy)])** (15:150:1) are obtained, respectively. Moreover, using the doping system of PVK:PBD:**[Ir(iqbt)$_2$(vb-ppy)]** or the **Poly(NVK-*co*-[Ir(iqbt)$_2$(vb-ppy)])** (150:1) doped with PBD and the grafting system of the bipolar **Poly((vinyl-PBD)-*co*-NVK-*co*-[Ir(iqbt)$_2$(vb-ppy)])** (15:150:1) as the EML, their reliable **NIR-PLEDs-I-III** are realized, respectively. Excitingly, for the **NIR-PLED-III** based on the bipolar **Poly((vinyl-PBD)-*co*-NVK-*co*-[Ir(iqbt)$_2$(vb-ppy)])** (15:150:1), the superior device performance (the η_{EQE}^{max} of 3.6% and the negligible

(< 5%) efficiency roll-off) renders bipolar Ir(III)-complex-grafted polymers a new platform to high-performance NIR-PLEDs.

Conflicts of interest

There are no conflicts to declare.

Acknowledgements

This work was funded by the National Natural Science Foundation (21373160, 21173165), the State Key Laboratory of Structure Chemistry (20190026), the Guangdong Basic and Applied Basic Research Foundation (2019A1515110527), the Wisteria Scientific Research Cooperation Special Project of Northwest University, the Hong Kong Research Grants Council (PolyU153058/19P), the Hong Kong Polytechnic University (1-ZE1C) and the Endowed Professorship in Energy from Ms. Clarea Au (847S) in China.

Notes and references

1 (a) L. T. Dou, Y. S. Liu, Z. R. Hong, G. Li and Y. Yang, *Chem. Rev.*, 2015, **115**, 12633-12665; (b) A. Rogalski and K. Chrzanowski, *Opto-Electron. Rev.*, 2002, **10**, 111-136.

2 J. Clark and G. Lanzani, *Nat. Photon.*, 2010, **4**, 438-446.

3 F. Ding, Y. Fan, Y. Sun and F. Zhang, *Adv. Healthcare Mater.*, 2019, **8**, 1900260.

4 (a) A. Zampetti, A. Minotto and F. Cacialli, *Adv. Funct. Mater.*, 2019, **29**, 1807623; (b) M. Ibahim-Ouali and F. Dumur, *Molecules*, 2019, **24**, 1412; (c) C.-L. Ho, H. Li and W.-Y. Wong, *J. Organomet. Chem.*, 2014, **751**, 261-285; (d) H. F. Xiang, J. H. Cheng, X. F. Ma, X. G. Zhou and J. J. Chruma, *Chem. Soc. Rev.*, 2013, **42**, 6128-6185.

5 J. H. Kim, J. H. Yun and J. Y. Lee, *Adv. Opt. Mater.*, 2018, **6**, 1800255.

6 (a) Y. X. Zhang, Q. Li,M.H. Cai, J. Xue and J. Qiao, *J. Mater. Chem. C*, 2020, **8**, 8484-8492; (b) J. Xue, L. J. Xin, J. Y. Hou, L. Duan, R. J. Wang, Y. Wei and J. Qiao, *Chem. Mater.*, 2017, **29**, 4775-4782; (c) I. Shigeru, Y. Shigeyuki, M. Takeshi, N. Hiroyuki, F. Hideki, K. Shiro and S. Yoshiaki, *Inorg. Chem. Commun.*, 2013, **38**, 14-19.

7 (a) Z. Chen, H. Y. Zhang, D. W. Wen, W. H. Wu, Q. G. Zeng, S. M. Chen and W.-Y. Wong, *Chem. Sci.*, 2020, **11**, 2342-2349; (b) C. F. You, D. H. Liu, M. B. Zhu, J. T. Yu, B. Zhang, Y. Liu, Y. F. Wang and W. G. Zhu, *J. Mater. Chem. C.*, 2020, **8**, 7079-7088; (c) C. F. You, D. H. Liu, F. Y. Meng, Y. F. Wang, J. T. Yu, S. Wang, S. J. Su and W. G. Zhu, *J. Mater. Chem. C.*, 2019, **7**, 10961–10971; (d) J. Zhou, G.R. Fu, Y. N. He, L. N. Ma, W. T. Li, W. X. Feng and X. Q. Lü, *J. Lum.*, 2019, **209**, 427-434; (e) H. U.Kim, S. Sohn, W. Choi, M. Kim, S. U. Ryu, T. Park, S. Jung and K. S. Bejoymohandas, *J. Mater. Chem. C.*, 2018, **6**, 10640-10658; (f) Y. Liu, Z. R. Han, F. Y. Meng, P. Wang, L. Yang, Y. F. Wang, Y. Pei and S. J. Su, *Chem. Phys. Lett.*, 2018, **699**, 99-106; (g) S. Kesarkar, W. Mróz, M. Penconi, M. Pasini, S. Destri, M. Cazzaniga, D. Ceresoli, P. R. Mussini, C. Baldoli, U. Giovanella and A. Bossi, *Angew. Chem. Int. Ed.*, 2016, **55**, 2714-2718; (h) X. S. Cao, J. S. Miao, M. R. Zhu, C. Zhong, C. L. Yang, H. B. Wu, J. G. Qin and Y. Cao, *Chem. Mater.*, 2015, **27**, 96-104; (i) R. Tao, J. Qiao, G. L. Zhang, L. Duan, C. Chen, L. D. Wang and Y. Qiu, *J. Mater. Chem. C.*, 2013, **1**, 6446-6454; (j) J. Qiao, L. Duan, L. T. Tang, L. He, L. D. Wang and Y. Qiu, *J. Mater. Chem.*, 2009, **19**, 6573-6580; (k) E. L.Williams, J. Li and G. E. Jabbour, *Appl. Phys. Lett.*, 2006, **89**, 083506.

8 (a) H. U. Kim, H. J. Jang, W. Choi, S. Park, T. Park, J. Y. Lee and K. S. Bejoymohandas, *J. Mater. Chem. C*, 2020, **8**, 4789-4800; (b) Y. N. He, G. R. Fu, W. T.Li, B. W. Wang, T. Z. Miao, M. F. Tan, W. X. Feng and X. Q. Lü, *J. Lum.,* 2020, **218**, 116847; (c) J. T. Yu, C. Xu, F. Y. Meng, H. Tan, M. Q. Liu and W. G. Zhu, *Dyes Pigm.*, 2019,**166**, 307-313; (d) Z. R. Hao, M. Li, Y. J. Liu, Y. F. Wang, G. H. Xie and Y. Liu, *Dyes Pigm.*, 2018, **149**, 315-322; (e) G. R. Fu, H. Zheng, Y. N. He, W. T. Li, X. Q. Lü and H. S. He, *J. Mater. Chem. C*, 2018, **6**, 10589-10596.

9 (a) L. J. Xin, J. Xue, G. T. Lei and J. Qiao, *RSC Adv.*, 2015, **5**, 42354-42361; (b) R. Tao, J. Qiao, G. L. Zhang, L. Duan, L. D. Wang and Y. Qiu, *J. Phys. Chem. C.*, 2012, **116**, 11658-11664.

10 J. V. Caspar and T. J. Meyer, *J. Phy. Chem.*, 1983, **87**, 952-957.

11 Y. M. Zhang, Y. F. Wang, J. Song, J. L. Qu, B. H. Li, W. G. Zhu and W.-Y. Wong, *Adv. Opt. Mater.*, 2018, **6**, 1800466.

12 F. Xu, H. U, Kim, J. Kim, B. J. Jung, A. C. Grimsdale and D. Hwang, *Prog. Polym. Sci.*, 2015, **47**, 92-121.

13 (a) Q. Zhao, S.-J. Liu and W. Huang, *Macromol. Rapid Commun.*, 2010, **31**, 794-807; (b) V. Marin, E. Holder, R. Hoogenboom and U. S. Schubert, *Chem. Soc. Rev.*, 2007, **36**, 618-635.

14 (a) C.-L. Ho and W.-Y. Wong, *Top. Curr. Chem.*, 2016, **374**, 1-23; (b) L. Ying, C.-L. Hong, H. B. Wu, Y. Cao and W.-Y. Wong, *Adv. Mater.*, 2014, *26*, 2459-2473.

15 M. Nonoyama, *Bull. Chem. Soc. Jpn.*, 1979, **52**, 3949-3750.

16 Z. Zhang, Y. L. He, L. Liu, X. Q. Lü, X. J. Zhu, W.-K. Wong, M. Pan and C. Y. Su, *Chem. Commun.*, 2016, **52**, 3713-3716.

17 J. K. Augustine, V. Vairperrumal, S. Narasimhan, P. Alagarsamy and A. Radhakrishnan, *Tetrahedron*, 2009, **65**, 9989-9996.

18 L. Liu, M. Y. Pang, H. T. Chen, G. R. Fu, B. N. Li, X. Q. Lü and L. Wang, *J. Mater. Chem. C*, 2017, **5**, 9021-9027.

19 P.-N. Lai, C. H. Brysacz, M. K. Alam, N. A. Ayoub, T. G. Gray, J. Bai and T. S. Teets, *J. Am. Chem. Soc.*, 2018, **140**, 10198-10207.

20 P.-N. Lai and T. S. Teets, *Chem. Eur. J.*, 2019, **25**, 6026-6037.

21 C. Tang, X. D. Liu, F. Liu, X. L. Wang, H. Xu and W. Huang, *Macromol. Chem. Phys.*, 2013, **241**, 314-342.

22 D. R. Martir and E. Zysman-Colman, *Coord. Chem. Rev.*, 2018, **364**, 86-117.

23 G. R. Fu, Y. N. He, W. T. Li, T. Z. Miao, X. Q. Lü, H. S. He, L. Liu and W.-Y. Wong, *Chem. Sci.*, 2020, **11**, 2640-2646.

24 G. R. Fu, L. Liu, W. T. Li, Y. N. He, T. Z. Miao, X. Q. Lü and H. S. He, *Adv. Opt. Mater.*, 2019, **7**, 1900776.

25 A. Kirch, M. Gmelch and S. Reineke, *J. Phys. Chem. Lett.*, 2019, **10**, 310-315.

26 Z.-H. Wang, H. Lee and H.-N. Cui, *J. Appl. Phys.*, 2012, **111**, 023512.

27 M. Mauro and C. Cebrian, *Israel J. Chem.*, 2018, **58**, 901-914.

28 (a) Z. R. Hao, H. G. Jiang, Y. Liu, Y. M. Zhang, J. T. Yu, Y. F. Wang, H. Tan, S. J. Su and W. G, Zhu, *Tetrahedron*, 2016, **72**, 8542-8549; (b) V. Jankus, K. Abdullah, G. C. Griffiths, C. Gareth, H. Al-Attar, Y. H. Zheng, M. R. Bryce and A. P. Monkman, *Org. Electron.*, 2015, **20**, 97-102; (c) H. Al-Attar, G. C. Griffiths, T. N. Tom, M. Tavasli, M. A. Fox, M. R. Bryce and A. P. Monkman, *Adv. Funct. Mater.*, 2011, **21**, 2376-2382.

29 (a) T. Y. Li, J. Wu, Z. G. Wu, Y. X. Zheng, J. L. Zuo and Y. Pan, *Coord. Chem. Rev.*, 2018, **374**, 55-92; (b) X. L. Yang, G. J. Zhou and W.-Y. Wong, *Chem. Soc. Rev.*, 2015, **44**, 8484-8575.

30 (a) T. Earmme and S. A. Henehke, *J. Mater. Chem. C*, 2012, **22**, 4660-4668; (b) T. L. Te, S. Y. Shao, J. S. Chem, L. X. Wang and D. G. Ma, *ACS Appl. Mater. Interfaces*, 2011, **3**, 410-416.